# Modulating outcomes of oil drops bursting at a water-air interface

Cite as: Appl. Phys. Lett. 125, 141601 (2024); doi: 10.1063/5.0216820 Submitted: 1 May 2024 · Accepted: 19 September 2024 · Published Online: 1 October 2024







Varun Kulkarni, 🛮 🕞 Suhas Tamvada, 🕞 Yashasvi Venkata Lolla, 🕞 and Sushant Anand 🗈 🅞





#### **AFFILIATIONS**

Department of Mechanical and Industrial Engineering, University of Illinois at Chicago, Chicago, Illinois 60607, USA

<sup>a)</sup>Authors to whom correspondence should be addressed: varun14kul@gmail.com and sushant@uic.edu

#### **ABSTRACT**

Recent studies have shown that capillary waves generated by the bursting of an oil drop at the water-air interface produces a daughter droplet inside the bath, while a part of it floats above it. Successive bursting events produce next generations of daughter droplets, gradually diminishing in size until the entire volume of oil rests atop the water-air interface. In this work, we demonstrate two different ways to modulate this process by modifying the constitution of the drop. First, we introduce hydrophilic clay particles inside the parent oil drop and show that it arrests the cascade of daughter droplet generation preventing it from floating over the water-air interface. Second, we show that bursting behavior can be modified by a compound water-oil-air interface made of a film of oil with finite thickness and design a regime map, which displays each of these outcomes. We underpin both of these demonstrations by theoretical arguments providing criteria to predict outcomes resulting therein. Finally, all our scenarios have a direct relation to control of oil-water separation and stability of emulsified solutions in a wide variety of applications, which include drug delivery, enhanced oil recovery, oil spills, and food processing, where a dispersed oil phase tries to separate from a continuous phase.

Published under an exclusive license by AIP Publishing. https://doi.org/10.1063/5.0216820

Dispersion of oil droplets in aqueous solutions are common in household items like salad dressings,1 ointments,2 and cosmetic creams<sup>3</sup> but even at larger scales in environment and industry such as oil spills<sup>4,5</sup> and enhanced oil recovery.<sup>6</sup> These interactions are characterized by either their ability to remain together as a homogeneous mixture or get separated as disparate oil and water phases. In this light, two major directions for research have emerged over the years: on the one hand, the focus has been on understanding the kinetics and enhancing stability of dispersed oil droplets in a continuous water phase,<sup>7–9</sup> while on the other hand, mechanisms for their separation have been investigated. Results from these findings have often found use in applications like emulsion synthesis 10 and dispersal of oil slicks modulated by surfactants, 11 microbes, 12 particles, 13 or the combination thereof.<sup>14</sup> While the role of chemical constitution and its symbiotic relationship with physical hydrodynamics in separation or homogenizing of oil-water mixtures using physio-chemical modifiers like surfactants or particles is known, 15,16 it is yet unclear whether purely hydrodynamic mechanisms, which rely only on interfacial forces, can be the main drivers of such two-phase interactions.

Along this line, the recent work by Kulkarni et al. 17 and Lolla. 18 has revealed a novel, unexplored pathway of oil separation from the surrounding water phase by investigating the bursting of a rising oil drop at an air-water interface. It was demonstrated that the bursting oil drop produces a daughter droplet within the continuous phase, and the process cascades down until the oil drop forms a film above the water-air interface. The significance of this may be readily appreciated, as leakages from broken underwater oil pipelines and natural seeps release oil droplet plumes where individual oil drops rise, 19 eventually bursting at the water-air interface, and this may even be encountered in two-phase microfluidic droplet-based flows. Quite naturally, methods to control this separation provide interesting avenues for future investigations, with profound implications.

In this work, we pursue this objective and demonstrate two specific methods to control and modify this behavior by manipulating the oil drop/water interface, which heretofore has only been shown by changing the viscosity of the water bath 17,18 (continuous phase). First, we show that hydrophilic bentonite (clay) particles mixed in an oil drop rising in a water bath can self-assemble at the oil-water interface to controllably halt successive bursting events. This situation resembles crude oil leaking from underwater pipeline bursts and entrains mineral/clay particles from the seafloor<sup>20–22</sup> or that seen in separation of Pickering emulsions.<sup>23</sup> Our second study is inspired by double emulsion synthesis and buoyant crude oil jets entrapping the surrounding water phase to form a water-in-oil compound drop.<sup>24</sup> We consider

bursting of such compound drops made of encapsulated water drops of varying diameters, which heretofore has only been investigated for oil-coated air bubbles<sup>25–27</sup> or falling drops.<sup>28</sup> By these simple modifications to the oil drop–water interface, we may regulate bursting outcomes such as cessation of bursting cascade at any given stage corresponding to a particular daughter droplet size and morphology of the daughter droplet produced.

For our experiments,  $^{17,18}$  we use hexadecane ( $\rho_o$ , 773 kg m<sup>-3</sup> and dynamic viscosity,  $\mu_o$ ,  $3 \times 10^{-3}$  Pa s) oil drops, insoluble in a D.I. (deionized) water bath ( $\rho_w$ , 998 kg m<sup>-3</sup> and dynamic viscosity,  $\mu_w$ ,  $1 \times 10^{-3}$  Pa s). In addition to its practical relevance, since water or hexadecane do not significantly dampen the capillary waves as in the case of more viscous outer liquids or typical two-fluid drop dynamics, <sup>29,30</sup> we choose them as the continuous (bulk) liquid and dispersed (drop) phase, respectively, to observe all subsurface phenomena clearly. The interfacial tension  $\sigma_{w/o}$  between hexadecane and water is 0.052 N m<sup>-1</sup>, and  $\mu_o$  of hexadecane is small enough for viscous effects to be neglected.4 Furthermore, hexadecane has a spreading coefficient of −0.0083 N m<sup>-1</sup> which makes it non-spreading, forming a lenticular shape above the water-air interface. Its spreading is also considered negligible since its timescale is much longer than that for the subsurface dynamics.<sup>31</sup> The experimental observations are recorded using videos<sup>4</sup> taken at 4500 fps and a resolution of  $1024 \times 1024$  pixels such that 1 pixel  $\approx 15 \,\mu\text{m}$ . The depth of the water bath is maintained such that when the drops are completely detached from the needle they continue to be completely submerged inside the water bath. Additional details of the experiments are presented below in the appropriate sections.

To investigate the effect of inclusion of particles on oil drop bursting at the water–air interface, a known initial weight,  $\phi \approx 3\%$  of

hydrophilic bentonite clay particles was introduced into the parent (p) oil (hexadecane) drop as illustrated in Fig. 1(a) (Multimedia view). The diameter of the clay (c) particles measured using SEM varied between 5 and 25  $\mu$ m with an average value  $\langle a_c \rangle$  of 15  $\mu$ m, where  $\langle \cdot \rangle$  stands for the average of particles of different sizes [see Fig. 1(b)]. The particle-laden oil drop is released from a 0.5 mm inner diameter nozzle producing a parent drop of radius  $R_p$  equal to 2.2 mm and volume of nearly 45  $\mu$ l. The bentonite clay particles are hydrophilic in nature  $^{32}$  and almost completed wetted by water due to which the oil–water interfacial tension (and surface energy) is not affected much and we only use them in weight percentages between 0 and 6%, which does not alter the overall oil drop density, significantly. Finally, these particles have low solubility in water but their negative surface charge is neutralized by it, depressing their zeta potential  $^{33}$  and not considered as a dominant factor in our analysis.

As the oil drop rises through water due to the hydrophilic nature of the clay particles they are expected to adsorb  $^{34}$  and self-assemble at the oil–water interface. To confirm this, we conducted two specific experiments. In our first study, we used confocal laser scanning microscopy (CLSM) with water labeled using a green fluorophore and clay particles using a red one. The self-assembly of the clay particles upon release of particle-laden oil drop to form a shell (red ring) encapsulating the drop surrounded by water is clearly visualized here and shown in Fig. 1(c-i) (taken mid-plane, cutting across the diameter of the drop). The enlarged view in Fig. 1(c-ii) shows details of part of the drop revealing the formation of a 20  $\mu$ m thick particle shell covering the oil drop of radius 1 mm.

To further confirm these observations, we conducted a second set of experiments in which we dispensed an oil drop containing clay

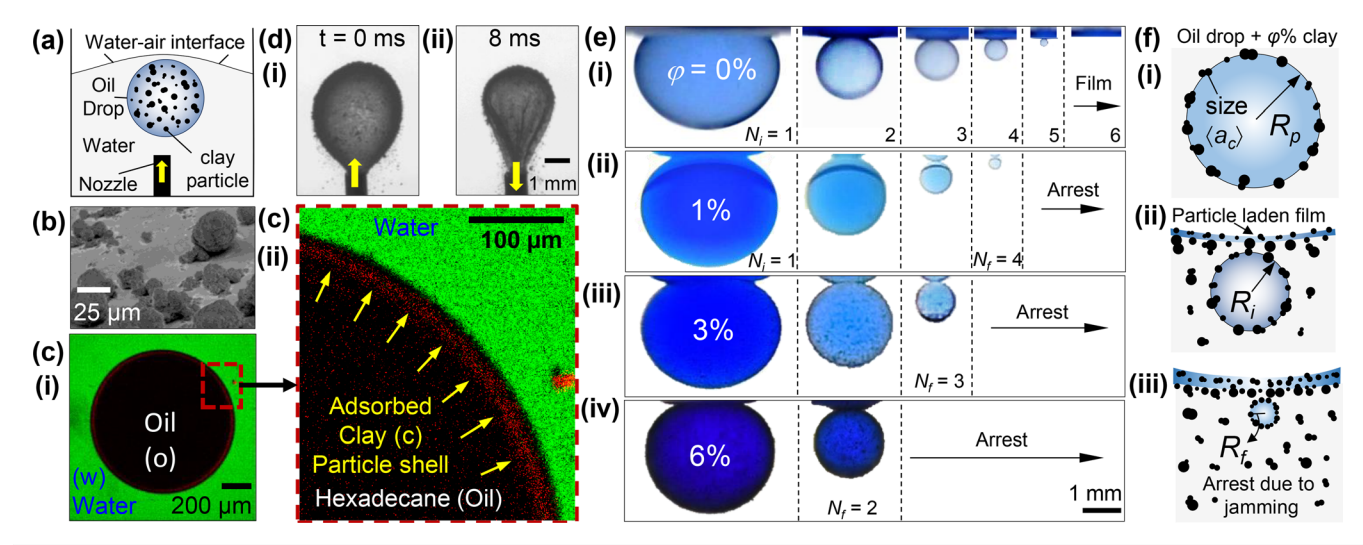


FIG. 1. (a) Schematic of experimental setup showing a rising oil drop containing bentonite clay particles bursting at an air–water interface after being released upward. (b) Scanning electron microscopy (SEM) image of bentonite clay particles with a median size of  $20~\mu m$ . (c-i) Confocal laser scanning microscope (CLSM) image of a hexadecane (oil) drop in water with adsorbed clay particles at the oil–water interface forming a shell. Clay particles and bulk water are labeled using Rhodamine-B fluorescent red dye and Fluorescein green dye, respectively, with hexadecane not being dyed (therefore, seen in black). (c-ii) Zoomed view of (c-i) showing the adsorption of particles at the oil–water interface. Yellow arrows show the shell of clay particles (dyed red). (d) Proof of self-assembly of clay particles demonstrated by (d-i) injecting a particle-laden oil drop into a bulk of water and, retracting the liquid (d-ii). Self-assembled particles adsorbed at the oil–water interface form a shell around the oil droplet, which crumples during retraction. Effect on cascade, (e-i) without particles, (e-ii)-(e-iv) with particles showing early cessation with increasing particle concentration,  $\varphi = 1\%$ , 3%, and 6%. (f) Mechanism of cascade arrest: (f-i) initial particle coverage, (f-ii) drop bursting leading to particle-laden oil film and daughter droplet generation with increased surface coverage below the interface, and (f-iii) formation of a *Pickering* drop with final arrest with 90% drop surface coverage of particles. Multimedia available online.

particles from a nozzle allowing the hydrophilic particles to selfassemble at the oil-water interface and form a shell as depicted in Fig. 1(d-i), t = 0 ms. Thereafter, we slowly retract oil from the nozzle and notice discernible creasing/crumpling of the interface after a few moments, at t = 8 ms [see Fig. 1(d-ii)], owing to the presence of the shell of clay particles. These above-mentioned results confirm selfassembly of solid layer of clay particles around the oil drop, enabling us to explore the effect of increasing  $\varphi$  on the bursting of hexadecane (oil) drops. To this end, we varied  $\varphi$  from 1 to 6 wt. % and recorded the number of bursting events  $N_f$  required to arrest the daughter droplet cascade. The sequence of images obtained from videos recorded from our experiments is shown in Figs. 1(e-i)-1(e-iv). The first row represents the case when particles were absent in the oil drop, and it is observed that after  $N_i = 5$ , the entire original parent oil drop formed a film (without clay particles) as reported in our previous work.<sup>17</sup> On introducing clay particles at increasing  $\varphi$  of 1%, 3%, and 6%, as shown in the second, third, and the fourth row, the cascade is arrested much earlier, at  $N_f = 4, 3$ , and 2, respectively, producing a particle covered drop, reminiscent of a Pickering drop of the anti-Bancroft type<sup>2</sup> each time, which was stable for at least 18h until the water bath completely evaporated.

In order to understand the underlying mechanism, we consider the particle-laden parent oil drop of radius  $R_p$  after it is released from the nozzle as portrayed schematically in Fig. 1(f-i) and denoted by the symbol  $N_i = 1$ , where the subscript i denotes the generation of daughter droplet, with i = 1 being the parent drop.

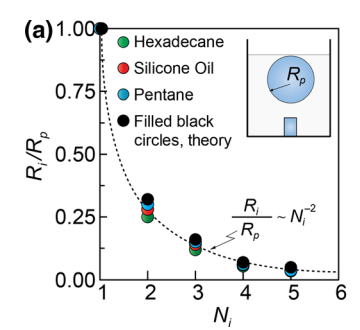
During the rise of the parent oil drop, clay particles preferentially self-assemble 15,35 along the water-oil interface with a certain initial surface coverage,  $\chi_1$  ultimately halting near the water–air interface. This is followed by bursting of thin bulk (b) water film between the oil drop and water-air interface producing a daughter droplet (of radius,  $R_i$ ) with higher intermediate particle surface coverage,  $\chi_i$  compared to the initial particle-laden parent drop and a thin layer particle-infused oil film atop the water-air interface as sketched in Fig. 1(f-ii). With subsequent bursting events  $(N_i > 1)$ , the daughter droplet size  $R_i$  continues to decrease with increasing  $\chi_i$ , eventually resulting in tight enough packing of particles (with coverage  $\chi_f$ ) on its drop/bulk interface at which stage  $(N_t)$  subsequent bursting is arrested. No more oil can drain through this particle shell at this stage, and bursting is jammed by the particle-infused oil film residing above [see Fig. 1(f-iii)]. Even though it might follow from (initial) the high value of  $\chi_1$  that bursting will not commence, such a configuration does not lead to stable oil-in-water emulsion, restricting  $\varphi$  to 0–6 wt. % (see Sec. 1 of the supplementary material for details and clay particle size distribution). Using the expression by Golemanov et al.,  $^{36}$   $\varphi$ =  $8\chi_1(\rho_c/\rho_o)/((2R_p/\langle a_c\rangle) + 8\chi_1(\rho_c/\rho_o-1))$  and plugging in values of  $\chi_1=0.9,\,\rho_c=2400\,\mathrm{kg\cdot m^{-3}},\,\rho_o=773\,\mathrm{kg\cdot m^{-3}},\,R_p=2.2\,\mathrm{mm},$  and  $\langle a_c\rangle=15\,\mu\mathrm{m}$  for anti-Bancroft emulsions, we obtain,  $\varphi\approx7\%$  for which a drop of radius 2.2 mm will be stable by itself. We have chosen a limit slightly below this value of 6% to ensure we continue to see at least one bursting event.

To make quantitative predictions about  $N_f = F(\varphi)$  based on the above mechanism, we note that until the formation of a final stable daughter droplet of radius,  $R_f$ , the bursting process is expected to be similar to the case when particles are absent [see Fig. 1(e-i)] since  $\chi_{i=1}$  is not large enough to cover the entire drop's surface initially. However, once  $\chi_i$  reaches  $\chi_f = 0.90$ , the cascade is arrested<sup>36</sup> by the

mechanism explained previously. We could use this to relate  $R_f$  with final number of particles  $n_{c,f}$  that it contains using the relation  $\chi_f = n_{c,f} \langle a_c \rangle^2 / 16 R_f^2$ . For a constant  $\langle a_c \rangle$  and  $\chi_f = 0.9$  (at arrest), we may write  $R_f^2 \sim n_{c,f}$ . From here, it only remains to connect  $n_{c,f}$  with  $\varphi$  and  $R_f$  with  $N_f$  to get the functional form of  $N_f$  in terms of  $\varphi$ .

In pursuit of the aforementioned, we first recognize  $\varphi = \rho_c \langle a_c \rangle^3 n_{c,i=1} / 8 \rho_o R_p^3$ , where  $n_{c,i=1}$  is the initial number of clay particles, and  $\rho_c \approx 2400 \, \mathrm{kg \, m^{-3}}$  is the density of the clay particles. Since  $R_p \approx 3.4 \, \mathrm{mm} \, \langle a_c \rangle$  and  $\rho_o$  are constants for our experiments, we obtain,  $\varphi \sim n_{c,1}$ . Moreover, larger  $\varphi$  requires larger  $R_f$  with a larger surface area  $\sim R_f^2$  (see previous paragraph) to accommodate all the particles; therefore, it is reasonable to expect  $\varphi \sim n_{c,1} \sim n_{c,f} \sim R_f^2$ , thereby simplifying our scaling relation to the form  $R_f^2 \sim \varphi$ .

Now, it only remains to connect the number of bursting events  $N_f$  required to arrest the cascade at a specific daughter droplet of radius  $R_f$ . To do so, we use the scaling relation derived in our previous work<sup>17</sup> for the daughter droplet size  $R_{i=2} \sim \zeta^{-2.34} R_b^{2.74}$ , where the constant  $\zeta = \mu_b / \sqrt{\rho_b \sigma_{pb}}$ . To obtain the daughter droplet size after the next bursting event  $N_i = 3$ , we substitute  $R_{i=2}$  from this scaling as  $R_p$  in the same expression. Recursively, this gives rise to  $R_{i=3} \sim \zeta^{-2.34(1+2.74)} R_p^{2.74^2}$ . Therefore, after  $N_i (\geq 2)$  cascades, we write the general expression for  $R_i$ , the daughter droplet size after  $N_i$  generations,  $R_i/R_p \sim \zeta^{-2.34\mathcal{M}} R_p^{2.74^{N_i-1}-1}$ , where  $\mathcal{M} = \sum_{i=1}^{N_i-1} 2.74^{i-1}$ . We use this expression to determine theoretically the variation of the daughter droplet size  $R_i/R_p$  with  $N_i$  for a given  $R_p \approx 3.4$  mm, which we see to match our experimental values accurately [see Fig. 2(a)]. However, this form is inconvenient to use for further analysis and, therefore, we seek a more concise functional dependence of the type,  $R_i/R_p = F(N_i)$ . To do so, we use a best fit curve to represent our experimentally and theoretically obtained values and obtain the relation  $R_i \sim R_p N_i^{-2}$ , which for a constant  $R_p \approx 3.4$  mm reads  $R_i \sim N_i^{-2}$ . This relation could alternatively even be obtained rigorously by expanding  $\zeta^{-2.34\mathcal{M}} R_p^{2.74^{N_i-1}-1}$  in Taylor series to obtain its polynomial form but not undertaken here for conciseness. At the arrest radius  $R_f$ this assumes the form  $R_f \sim N_f^{-2}$ , obtained by setting i = f in



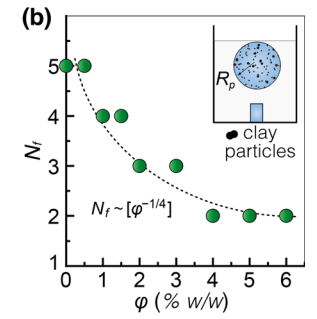


**FIG. 2.** (a) Ratio of daughter droplet  $R_i$  to parent drop radius  $R_p$  at each bursting event  $N_i$  in the absence of particles in three oil drops (hexadecane, silicone oil, and pentane) <sup>17</sup> yielding the scaling relationship  $R_f/R_p \sim N_i^{-2}$ . (b) Decrease in the number of bursting events required to arrest the cascade  $N_f$  with increasing clay particle concentration  $(\varphi)$  in the oil drop, exhibiting a scaling dependence of the form  $N_f \sim [\varphi^{-1/4}]$ . Refer Figs. 1(e) and 1(f) for symbols used here.

 $R_i \sim N_i^{-2}$ . Finally, we combine this scaling relation with  $R_f^2 \sim \varphi$ , which gives the number of bursting events or cascades  $N_{i=f}$  before arrest at an initially prescribed  $\varphi$  as

$$N_f \sim \left[ \phi^{-1/4} \right]. \tag{1}$$

In Eq. 1,  $[\cdot]$  is the nearest integer function, and the scaling obtained accurately predicts the data as shown in Fig. 2(b) with a scaling prefactor evaluated as 1.2±0.03. We also state that the scaling relation [Eq. (1)] remains unchanged for any particle size distribution (see Sec. S1 of the supplementary material) or any initial parent drop radius  $R_p$  as it algebraically cancels out leading to Eq. (1).

Our results so far show that the solid shell of particles provide an attractive route to modify post-bursting outcomes. Encouraged by these findings, we examine the consequence of bursting at an air-water interface when a liquid shell of variable thickness surrounds the oil drop as rationalized by a water-in-oil-compound drop. To study this, we use a coaxial nozzle of inner diameter 0.56 mm and annular gap of 1.7 mm, producing a compound drop parent drop of radius,  $R_p = 2.2 \,\mathrm{mm}$  and volume  $V_p$  with varying water (w) drop radius  $R_w$  (0.5–2.1 mm) and volume,  $V_w$ . Such an arrangement produces an oil (o) layer of thickness,  $h_o$ and volume  $V_o$  as shown schematically in Fig. 3(a), which subjects the bulk (water) and oil layer inside to continual drainage (see Sec. S2 of the supplementary material). Three volume fractions  $V_r := V_w/V_o$ , which corresponds to  $V_r \ll 1$ ,  $V_r \gg 1$ , and  $0.04 < V_r < 40$  of the compound drops are tested whose dependence on dimensionless oil layer thickness  $h_o/R_w$  is shown in Fig. 3(b). For these calculations, we compute  $V_r$  as  $R_w^3/(R_p^3-R_w^3)$ . Considering  $R_p=R_w+h_o$ , we can rewrite  $V_r$  as  $[(h_0 R_p^2/R_w^3)(1 + R_w/R_p + R_w^2/R_p^2)]^{-1}$ . In the limit,  $V_r \ll 1$  and  $V_r \gg 1$ , this reduces to  $h_o/R_w \approx V_r^{-1/3}$  and  $h_o/R_w \approx \frac{1}{3} V_r^{-1}$ , respectively (more details of this algebra may be found in Sec. S3 of the supplementary material).

Our experimental results at different  $V_r$  are shown in Figs. 3(c)–3(e), Multimedia view. At low  $V_r(\ll 1)$ , once the parent compound drop bursts, capillary waves descend downward, pinching the drop to form a daughter droplet, which encapsulates the original water drop within [see Fig. 3(c)]. In emulsion synthesis where excess material removal has been typically achieved through solvent evaporation, <sup>38,39</sup> this could provide a facile solution strategy. At intermediate  $0.04 < V_r < 40$ , the encapsulated water drop is large enough to suppress daughter droplet formation altogether as shown in Fig. 3(d) and the drop just floats up eventually. Finally, at large  $V_r(\gg 1)$ , the thin oil film surrounding the water drop bursts at the bulk water–air interface producing sub-surface polydispersed oil droplets [see Fig. 3(e)] bearing similarities to bursting of curved thin liquid films <sup>40,41</sup> and those produced by raindrop impacts on oil slicks.

To mathematically determine when each of these regimes will be observed, we develop a design map based on our experimental data as shown in Fig. 4. Our arguments follow from the premise that rising water-in-oil compound drops experiences two competing drainage flows whose timescales are determined by Stefan–Reynolds theory<sup>43</sup> (see Sec. S2 of the supplementary material). At  $V_r \ll 1$ , the timescale of drainage  $\sim \mu_o R_w^4/F_{w/o}h_o^2$  of the oil layer  $(h_o \gg R_w)$  due to apparent weight  $(F_{w/o})$  of the encapsulated water drop within the oil (parent, hexadecane) drop given by  $(\rho_w - \rho_o)V_wg + \rho_wV_pg$  (where g = 9.81 m·s<sup>-2</sup> is the gravitational acceleration) is required to be greater than the timescale  $\sim \mu_w R_p^4/F_{p/b}h_p^2$  of buoyancy driven squeezing of bulk water film of thickness  $h_p$  driven by the force  $F_{p/b} = (\rho_w - \rho_o)V_pg$  to

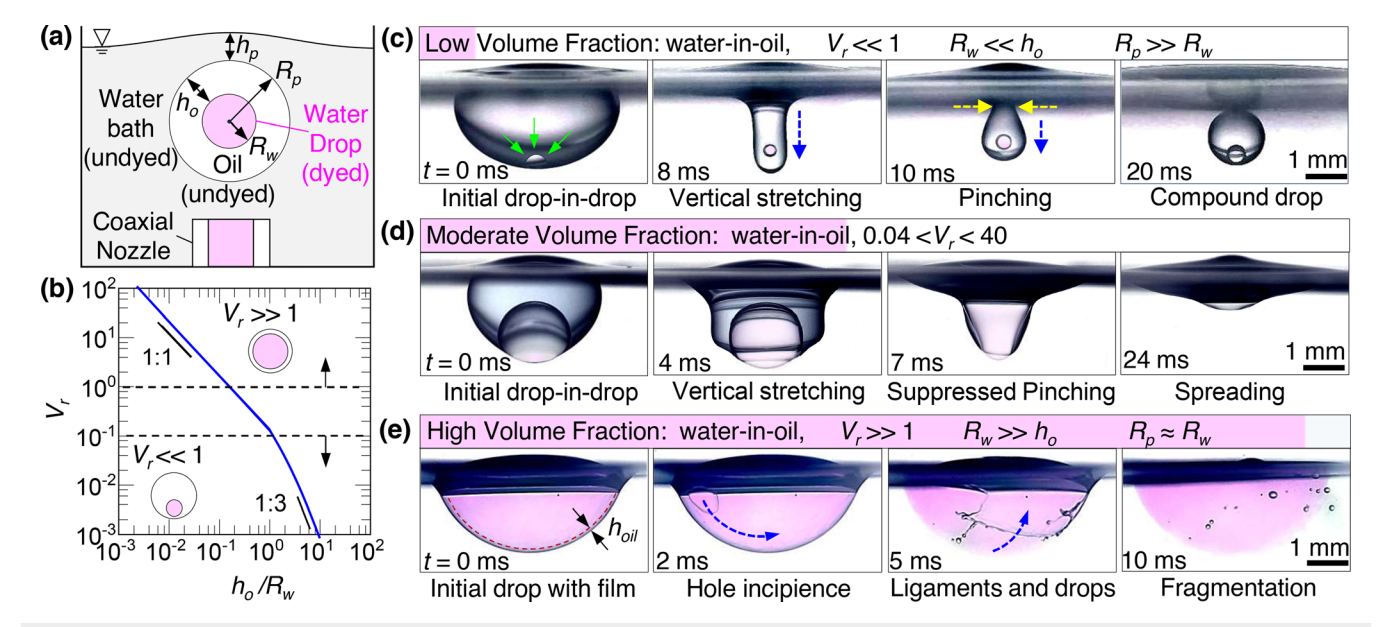


**FIG. 3.** (a) Schematic shows a rising water-in-oil compound drop generated using a co-axial nozzle. The inner water drop is dyed pink using rhodamine D while the water bath and the oil covering it are not. (b) Dependence of volume ratio,  $V_r$  of water-in-oil in a compound drop on the ratio of oil film thickness and water drop radius  $h_o/R_w$ . In the limit  $V_r \ll 1$ , it reduces to  $V_r \approx (h_o/R_w)^{1/3}$ , and for  $V_r \gg 1$ , it yields,  $V_r \approx (3h_o/R_w)^{-1}$ . Bursting process of a compound drop (c) at low  $V_r \approx 5\%$  (green arrows, the initial encapsulated water drop), producing an encapsulated daughter water drop of higher  $V_r$  (dotted arrows, movement direction) (d) at intermediate  $0.04 < V_r < 40$  with suppression of daughter droplet production (e) at high  $V_r \approx 97\%$ , leading to underwater oil film fragmentation (dotted arrows, hole expansion direction) and polydispersed daughter oil droplets. Note, waves after bursting approximately travel a distance of  $1.5\pi R_p$  to cover the entire drop. Multimedia available online.

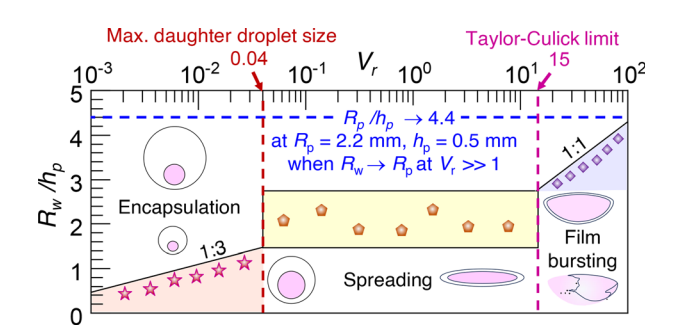


**FIG. 4.** Design map predicting encapsulation, spreading, and film bursting at different dimensionless water drop radius  $R_{\rm w}/h_{\rm p}$  as a function of  $V_{\rm r}$  for  $R_{\rm p}=2.2$  mm. Symbols are experimental data.

ensure the water drop remains inside the compound daughter droplet after bursting. This condition leads us to the balance  $(\rho_r-1)(2\rho_r V_r-V_r+\rho_r)^{-1}\sim \mu_r(h_o^2/R_w^2)(R_w^2/h_p^2)$  at the regime boundary, where  $\rho_r:=\rho_w/\rho_o$  and  $\mu_r:=\mu_w/\mu_o$ . Using the geometric approximation  $h_o/R_w\approx V_r^{-1/3}$  [see Fig. 3(b)] and algebraic simplification  $2\rho_r V_r-V_r+\rho_r\approx \rho_r$  for  $V_r\ll 1$  (see Secs. S3 and S4 of the supplementary material) and considering that the fluid properties  $(\rho_r=1.2,\mu_r=3,$  and  $R_p=2.2$  mm) are a constant, we arrive at the following simplified relation for the boundary of encapsulation,

$$R_w/h_D \sim V_r^{1/3}$$
. (2)

Similarly, to derive the criterion of film bursting at  $V_r\gg 1$ , the time-scale of drainage of the *thin* oil film  $(h_o\ll R_w)$  due to dominant interfacial tension or capillarity (cap),  $F_{\rm cap}=\sigma_{w/o}(2\pi R_p)$  should be greater than the buoyancy driven drainage due to force  $F_{p/b}$  described earlier, which at the regime boundary reads  $F_{p/b}/F_{\rm cap}\sim \mu_r h_o^2/h_p^2$ . This simplifies to  $(\rho_r-1)(2/3)[(\rho_r-1)(1+V_r)]^{-1}(Bo_{w/o})\sim \mu_r h_o^2/h_p^2$ , where  $Bo_{w/o}=(\rho_w-\rho_o)R_p^2g/\sigma_{w/o}$ . Like earlier, fluid properties  $\mu_r,\,\rho_r,\,$  and  $R_p$  are a constant, which along with the geometric approximation  $h_o/R_w\approx (3V_r)^{-1}$  [see Secs. S3 and S4 of the supplementary material and Fig. 3(b)] yields at the transition boundary,

$$R_w/h_p \sim V_r.$$
 (3)

For closure, we evaluate three more bounds for  $R_p \approx 2.2$  mm: (I) since lubrication flow approximation is valid for Reynolds number  $Re_b = \rho_w v_w h_p / \mu_w \ll 1$ , for a rise velocity  $v_w \approx 0.002$  m/s (from experiments), we obtain  $h_p = 0.5$  mm, which results in  $R_p / h_p \approx 4.4$ . Note that maximum value attained by  $R_w / h_p$  is when the encapsulated water drop occupies the entire volume of the compound drop, at  $V_r \gg 1$ , equivalent to  $R_w \to R_p$  and, therefore,  $R_w / h_p = R_p / h_p \approx 4.4$ . (II) To ensure complete encapsulation after bursting, we require  $R_w \leq R_{i=2} = R_p / 2^2$ , where  $R_2$  is the daughter droplet radius after the first bursting event (see Fig. 2). For  $h_o / R_w \approx V_r^{-1/3}$  at  $V_r \ll 1$  and  $h_o / R_w \approx R_p / R_w$ , this results in  $V_r \approx 0.04$ . (III) Finally, at  $V_r \gg 1$ , the oil film transitions from capillary dominated dynamics at moderate  $V_r$  at a timescale  $r_{mod} = (\rho_o R_p^3 / \sigma_{w/o})^{0.5}$ , with capillary waves traveling a distance of  $\approx 1.5\pi R_p$  at an average velocity scale  $v_{mod} / 2 = 1.5\pi R_p / \tau_{mod}$  [see Fig. 3(e)] to bursting of a curved film  $r_v$  at higher  $r_v$ , with an expanding hole retracting at the Taylor–Culick velocity

 $v_{tc} = (2\sigma_{w/o}/\rho_o h_o)^{0.5}$ . For a smooth crossover,  $v_{tc}$  equals  $v_{mod}$ , which simplifies to  $h_o/R_p = (9\pi^2/2)^{-1}$ . On using the geometric approximation  $V_r \approx (3h_o/R_w)^{-1}$  for  $V_r \gg 1$  and  $R_w \approx R_p$ , we ultimately obtain the bound  $V_r \approx 15$ . The limits (I), (II), and (III) (see Sec. S4 of the supplementary material for details) along with Eqs. (2) and (3) shown in Fig. 4 complete the design map.

In summary, we show two ways to tailor consequence of a bursting oil drop at an air-water interface. First, we introduce hydrophilic clay particles inside the oil drop to arrest daughter droplet generation and, second, we encapsulate a water droplet inside an oil drop to find distinct behaviors at various water to oil volume fractions. The former of our demonstrations is directly connected to practical situations like entrainment of clay particles from the ocean bed in underwater oil pipeline bursts and Pickering emulsions. The latter is inspired by water encapsulation in buoyant oil jets, optimizing size of double emulsions and raindrop impact on oil slicks. In practical scenarios as seen in oceans and seas, we expect humidity, temperature, surfactants, and other contaminants to be present.<sup>4</sup> These can delay or accelerate the bursting processes but not prevent their observance altogether as reported in our work. Hence, we do expect our results to be relevant in normal marine climatic conditions and serve as guide for any future detailed investigations. In addition to oceanic/atmospheric sciences and colloidal synthesis for drug delivery/food/cosmetics, applications that benefit from ingenious manipulation of the consequences of bursting drops could also find our results useful.

See the supplementary material for (i) the consequences of high initial particle coverage in arresting daughter droplet formation and the effect of particle size distribution and (ii) additional details of algebra leading to the scaling inequalities (2) and (3) along with bounds, I, II, and III.

Financial support for this project through the NSF (EAGER) Award No. 2028571 is gratefully acknowledged. The authors thank Navid Saneie for his assistance in obtaining the SEM image of bentonite clay particles.

# AUTHOR DECLARATIONS Conflict of Interest

The authors have no conflicts to disclose.

#### **Author Contributions**

Varun Kulkarni: Conceptualization (equal); Data curation (equal); Formal analysis (equal); Funding acquisition (supporting); Investigation (equal); Methodology (lead); Project administration (equal); Software (equal); Supervision (equal); Validation (lead); Visualization (equal); Writing – original draft (lead); Writing – review & editing (lead). Suhas Tamvada: Data curation (equal); Formal analysis (equal); Investigation (lead); Software (lead); Validation (supporting); Visualization (equal); Writing – review & editing (equal). Yashasvi Venkata Lolla: Data curation (equal); Formal analysis (equal); Investigation (equal); Writing – review & editing (supporting). Sushant Anand: Conceptualization (equal); Funding acquisition (lead); Project administration (equal); Resources (lead); Supervision (equal); Writing – review & editing (equal).

#### **DATA AVAILABILITY**

The data that support the findings of this study are available from the corresponding authors upon reasonable request.

#### REFERENCES

- <sup>1</sup>N. N. Nikolova, C. D. M. Narváez, L. Hassan, R. A. Nicholson, M. W. Boehm, S. K. Baier, and V. Sharma, "Rheology and dispensing of real and vegan mayo: The chickpea or egg problem," Soft Matter 19, 9413–9427 (2023).
- <sup>2</sup>A. Takamura, F. Ishii, S. Noro, and M. Koishi, "Physicopharmaceutical characteristics of an oil-in-water emulsion-type ointment containing diclofenac sodium," J. Pharm. Sci. 73, 676–681 (1984).
- <sup>3</sup>T. F. Tadros, "Future developments in cosmetic formulations," Int. J. Cosmetic Sci. 14, 93–111 (1992).
- <sup>4</sup>V. Kulkarni, V. Y. Lolla, S. R. Tamvada, N. Shirdade, and S. Anand, "Coalescence and spreading of drops on liquid pools," J. Colloid Interface Sci. 586, 257–268 (2021).
- <sup>5</sup>V. Kulkarni, V. Lolla, and S. Anand, "Oil droplet wetting dynamics on immiscible liquid surfaces," in APS Division of Fluid Dynamics Meeting Abstracts, 2018, Vol. 63.
- <sup>6</sup>A. Mandal, A. Samanta, A. Bera, and K. Ojha, "Characterization of oil-water emulsion and its use in enhanced oil recovery," Ind. Eng. Chem. Res. 49, 12756–12761 (2010).
- <sup>7</sup>R. P. Borwankar, L. A. Lobo, and D. T. Wasan, "Emulsion stability-kinetics of flocculation and coalescence," Colloids surfaces **69**, 135–146 (1992).
- <sup>8</sup>I. F. Guha, S. Anand, and K. K. Varanasi, "Creating nanoscale emulsions using condensation," Nat. Commun. 8, 1371 (2017).
- <sup>9</sup>Y. Liu and L. Yobas, "Microfluidic emulsification through a monolithic integrated glass micronozzle suspended inside a flow-focusing geometry," Appl. Phys. Lett. **106**, 174101 (2015).
- <sup>10</sup>Q. Wu, C. Yang, J. Yang, F. Huang, G. Liu, Z. Zhu, T. Si, and R. X. Xu, "Photopolymerization of complex emulsions with irregular shapes fabricated by multiplex coaxial flow focusing," Appl. Phys. Lett. 112, 071601 (2018).
- <sup>11</sup>Y. Kuang, T. Deng, Y. Huang, L. Liu, and G. Chen, "Droplet pair breakup in microfluidic expansion channel," Appl. Phys. Lett. 124, 034102 (2024).
- <sup>12</sup>U. U. Ghosh, H. Ali, R. Ghosh, and A. Kumar, "Bacterial streamers as colloidal systems: Five grand challenges," J. Colloid Interface Sci. 594, 265–278 (2021).
- <sup>13</sup>Z. Liu, Y. Zhang, T. Yang, Z. Wang, and H. C. Shum, "Compressed liquid marble ruptures at edge," Appl. Phys. Lett. 114, 243701 (2019).
- <sup>14</sup>W. Li, Y. Yu, D. Xiong, Z. Qi, W. Wang, and Y. Qi, "Effects of oil properties on the formation of oil-particle aggregates at the presence of chemical dispersant in baffled flask tests," J. Hazard. Mater. 436, 129227 (2022).
- 15T. Ngai and S. A. Bon, Particle-Stabilized Emulsions and Colloids: Formation and Applications (Royal Society of Chemistry, 2014).
- <sup>16</sup>S. Anand, V. Galavan, and M. U. Mulik, "Continuous synthesis of nanoscale emulsions by vapor condensation (EVC)," Adv. Sci. 11, 2307443 (2024).
- <sup>17</sup>V. Kulkarni, V. Y. Lolla, S. Tamvada, and S. Anand, "Bursting of underwater oil drops," Phys. Rev. Lett. 133, 034004 (2024).
- 18 V. Y. Lolla, "Dynamics of dewetting on a liquid substrate," M.S. thesis (University of Illinois at Chicago, 2019).
- 19Q. Wang, Y. Lü, L. He, X. Huang, and J. Feng, "Simulating oil droplet underwater dispersal from a condensate field spill in the south china sea," Ocean Eng. 284, 115090 (2023).
- <sup>20</sup>J. R. Payne, J. R. Clayton, Jr., and B. E. Kirstein, "Oil/suspended particulate material interactions and sedimentation," Spill Sci. Technol. Bull. 8, 201–221 (2003).
- <sup>21</sup>P. Hill, A. Khelifa, and K. Lee, "Time scale for oil droplet stabilization by mineral particles in turbulent suspensions," Spill Sci. Technol. Bull. 8, 73–81 (2002).

- <sup>22</sup>A. Khelifa, P. Stoffyn-Egli, P. S. Hill, and K. Lee, "Characteristics of oil droplets stabilized by mineral particles: Effects of oil type and temperature," Spill Sci. Technol. Bull. 8, 19–30 (2002).
- <sup>23</sup>R. Zheng and B. P. Binks, "Pickering emulsions stabilized by polystyrene particles possessing different surface groups," Langmuir 38, 1079–1089 (2022).
- <sup>24</sup>X. Xue and J. Katz, "Formation of compound droplets during fragmentation of turbulent buoyant oil jet in water," J. Fluid Mech. 878, 98–112 (2019).
- 25B. Ji, L. Hong, J.-T. Kim, L. P. Chamorro, and J. Feng, "Dynamics of an oil-coated bubble rising in a quiescent water medium," Phys. Rev. Fluids 7, 033603 (2022).
- <sup>26</sup>Z. Yang, B. Ji, J. T. Ault, and J. Feng, "Enhanced singular jet formation in oil-coated bubble bursting," Nat. Phys. 19, 884–890 (2023).
- <sup>27</sup>Z. Yang, B. Ji, and J. Feng, "Daughter oil droplet entrainment by oil-coated bubble bursting," J. Fluid Mech. 977, A10 (2023).
- <sup>28</sup>H. Deka, G. Biswas, K. C. Sahu, Y. Kulkarni, and A. Dalal, "Coalescence dynamics of a compound drop on a deep liquid pool," J. Fluid Mech. 866, R2 (2019).
- <sup>29</sup>M. R. Rahman, H. N. Mullagura, B. Kattemalalawadi, and P. R. Waghmare, "Droplet spreading on liquid-fluid interface," Colloids Surf., A 553, 143–148 (2018).
- 30 M. R. Rahman and P. R. Waghmare, "Influence of outer medium viscosity on the motion of rolling droplets down an incline," Phys. Rev. Fluids 3, 023601 (2018).
- <sup>31</sup>S. R. Tamvada, "Partial coalescence of oil and water: Spreading behavior and material synthesis," M. S. thesis (University of Illinois at Chicago, 2020).
- <sup>32</sup>S. Abend and G. Lagaly, "Bentonite and double hydroxides as emulsifying agents," Clay Miner. 36, 557–570 (2001).
- 33W. Huang, Y.-K. Leong, T. Chen, P.-I. Au, X. Liu, and Z. Qiu, "Surface chemistry and rheological properties of API bentonite drilling fluid: pH effect, yield stress, zeta potential and ageing behaviour," J. Pet. Sci. Eng. 146, 561–569 (2016).
- 34A. Yadav, E. J. Hinch, and M. S. Tirumkudulu, "Capillary-induced motion of particles bridging interfaces of a free-standing thin liquid film," Phys. Rev. Lett. 122, 098001 (2019).
- 35B. P. Binks and T. S. Horozov, Colloidal Particles at Liquid Interfaces (Cambridge University Press, 2006).
- <sup>36</sup>K. Golemanov, S. Tcholakova, P. Kralchevsky, K. Ananthapadmanabhan, and A. Lips, "Latex-particle-stabilized emulsions of anti-bancroft type," Langmuir 22, 4968–4977 (2006).
- <sup>37</sup>G. R. Blake, "Particle density," in *Encyclopedia of Soil Science*, edited by W. Chesworth (Springer Netherlands, Dordrecht, 2008) pp. 504–505.
- <sup>38</sup>T. Sheth, S. Seshadri, T. Prileszky, and M. E. Helgeson, "Multiple nanoemulsions," Nat. Rev. Mater. 5, 214–228 (2020).
- 39 A. Vian, B. Reuse, and E. Amstad, "Scalable production of double emulsion drops with thin shells," Lab Chip 18, 1936–1942 (2018).
- <sup>40</sup>V. Kulkarni, N. Shirdade, N. Rodrigues, V. Radhakrishna, and P. E. Sojka, "On interdependence of instabilities and average drop sizes in bag breakup," Appl. Phys. Lett. 123, 024101 (2023).
- <sup>41</sup>V. Kulkarni and P. E. Sojka, "Bag breakup of low viscosity drops in the presence of a continuous air jet," Phys. Fluids 26, 072103 (2014).
- <sup>42</sup>D. W. Murphy, C. Li, V. d'Albignac, D. Morra, and J. Katz, "Splash behaviour and oily marine aerosol production by raindrops impacting oil slicks," J. Fluid Mech. 780, 536–577 (2015).
- <sup>43</sup>A. Nguyen, "Historical note on the Stefan–Reynolds equations," J. Colloid Interface Sci. 231, 195 (2000).
- <sup>44</sup>H. Lhuissier and E. Villermaux, "Bursting bubble aerosols," J. Fluid Mech. 696, 5–44 (2012).
- 45). Zinke, E. D. Nilsson, P. Zieger, and M. E. Salter, "The effect of seawater salinity and seawater temperature on sea salt aerosol production," J. Geophys. Res. 127, e2021JD036005, https://doi.org/10.1029/2021JD036005 (2022).

# SUPPLEMENTARY MATERIAL

# Modulating outcomes of oil drops bursting at a water-air interface

Varun Kulkarni\*, Suhas Rao Tamvada¹, Venkata Yashasvi Lolla¹, Sushant Anand†,¹

<sup>1</sup>Department of Mechanical and Industrial Engineering, University of Illinois at Chicago, IL 60607 \*Corresponding author's email address: varun14kul@gmail.com †Corresponding author's email address: sushant@uic.edu

# Contents

| S1 Reasons for limiting particle weight % to $\varphi = 6\%$   | <b>2</b> |
|--|----------|
| S1.1 Effect of particle size distribution on scaling relation, $N_f \sim [\varphi^{-1/4}]$ , Eq. (1) in manuscript | 3        |
| S2 General considerations for film drainage in compound drops  | 4        |
| S2.1 Drainage of liquid between two applied forces   | 4        |
| S3 Relation between forces and geometric variables   | 5        |
| S3.1 Magnitude of various forces   | 6        |
| S3.2 Relation between $h_0, R_w$ and, $V_r$  |          |
| S3.2.1 Simplification when $V_r \ll 1$   |          |
| S3.2.2 Simplification when $V_r >> 1$  |          |
| S4 Criteria delimiting regimes of encapsulation, spreading and film bursting                                       | 8        |
| S4.1 Derivation of scaling boundary, (A), $R_w/h_p \sim V_r^{1/3}$   | 9        |
| S4.2 Derivation of scaling boundary, (B), $R_w/h_p \sim V_r$   |          |
| S4.3 Derivation of boundary (C), $V_r \approx 0.04$ , Daughter droplet generation limit                            |          |
| S4.4 Derivation of boundary ( <b>D</b> ), $V_r \approx 15$ , Taylor-Culick velocity limit                          |          |
| S4.5 Derivation of boundary (E), $R_{\rm sn}/h_{\rm rs} \rightarrow 4.4$   |          |

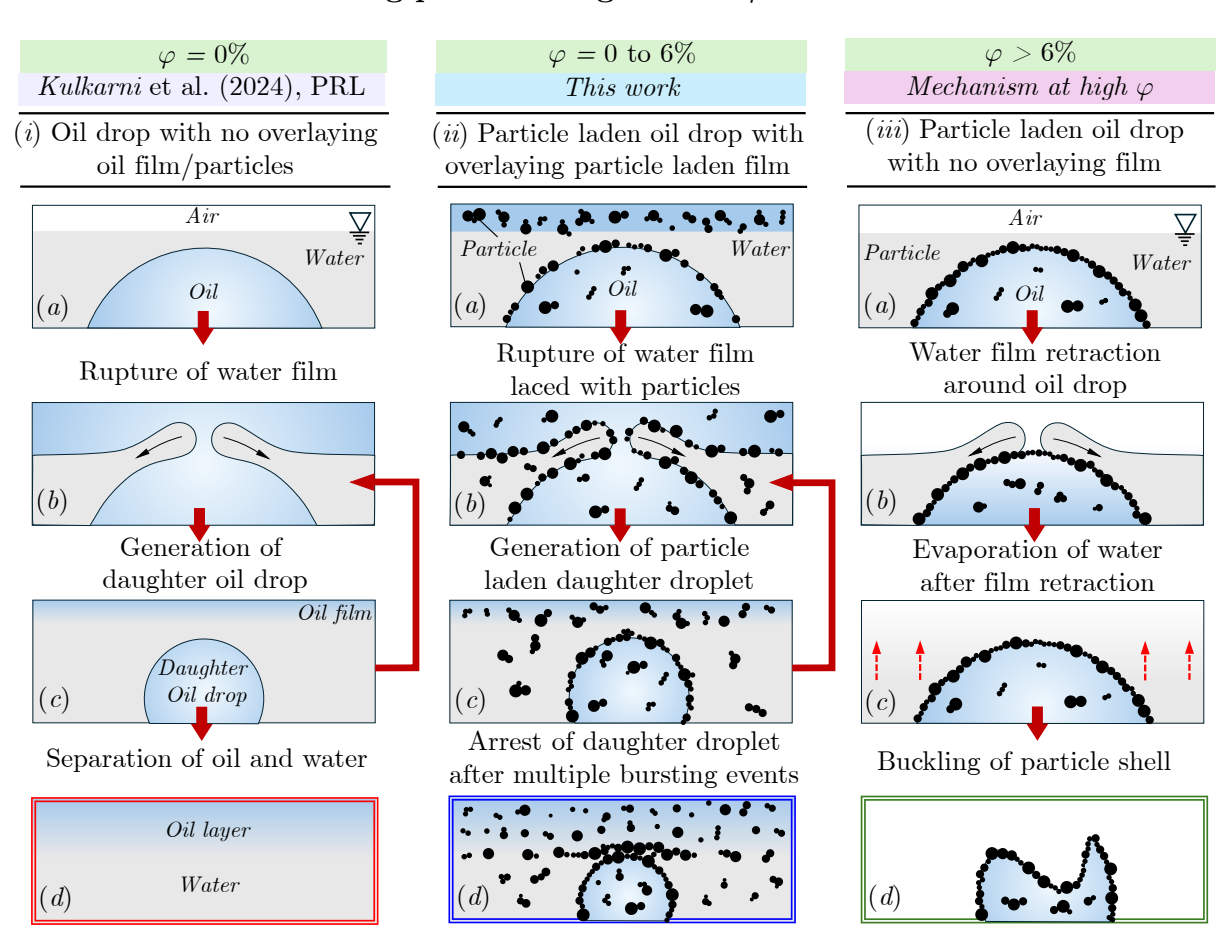


Figure S1: Schematic representations of three cases (i) Oil drop with and overlaying oil film without any particles, Kulkarni et al, 2024 [1] (a) Initial position of the oil drop as it rests near the water-air interface with the water slowly draining between the air and oil drop (b) Rupture of the water film followed by its retraction and generation of capillary waves (c) Separation of oil film from parent oil drop which repeats itself (as marked by maroon arrows) (d) Finally leading to entire separation of oil from water as a film floating over it. (ii) Particle laden oil drop with a overlaying particle laden oil film, THIS STUDY (a) Initial position of the oil drop laden with particles in the oil film above and surface coverage less than 0.90 to prevent tight packing (b) Rupture of water film bounded by particles on water-oil interface (c) Formation of two separate entities from the parent particles infused drop - an oil infused film and an particle infused oil drop (d) Final stage and arrest of drop due to particle laden oil film on top and tight packing around the oil drop (iii) Particle laden oil drop with no overlaying oil film (a) Tight packing which disallows draining of the oil from the drop (b) Retraction of water film over the particle infused oil drop (c) Evaporation (shown by dotted red arrows) of water surrounding particle laden drop (d) Buckling of particle shell in the final stages. It is important to note that despite tight packing a stable oil-water emulsion is not guaranteed in this configuration.

• Cause of cessation of bursting : Role of particle in the oil drop and the overlaying particle laden layer at  $0<\varphi<6~\%$ 

As the bursting commences two distinct fluid entities are created – one is the oil drop itself and the other is an oil on top. The stage-wise transition as the parent oil drop approaches the water-air interface and forms a daughter droplet is depicted in Fig. S1(i) (a)-(d). This follows from our earlier findings on such systems as reported in Kulkarni et al. [1].

In our current work this is extended to water-oil drop systems where the parent oil drop is infused with hydrophilic clay particles in an attempt to emulate conditions in a typical anti-Bancroft emulsion. Figure S1 (ii)(a)-(d) shows schematically the sequence of events followed once such a particle infused oil drops initially at rest (see Fig. S1(ii)(a)) is deformed by capillary waves. The rupture in this case follows the same dynamics as the one without particles (see Fig. S1(i)(b)) especially since the surface particle coverage is less than required for tight packing on the oil drop. This leads to the formation of

a daughter droplet as shown in Fig. S1 (ii)(c) with particles lacing its boundary and an oil film (with particles) above. The presence of particles in both the oil layer above and the daughter droplet is crucial to arrest to final daughter droplet formed after successive bursting events as shown in Fig. S1(ii)(d). The significance of this lies in the fact that the particle laden oil layer above prevents further cascade by arresting any water film drainage and the tight packing on the oil drop prevents any oil drainage that may lead to subsequent size reduction. So both are equally important.

#### • High particle weight fraction, $\varphi > 6\%$

For Pickering emulsions, a surface packing with a surface coverage of 0.9 or more is considered tight enough to prevent drainage of dispersed medium (in our case, oil) into the continuous medium (in our case water). This brings to light the possibility that the tight packing of the particles at the oil dropwater interface can arrest cascade and prevent production of further generations of daughter droplets. To understand what happens next, we refer to the steps outlined in Fig. S1(iii)(a)-(d). As water gradually drains above the particle infused oil drop at rest initially (see Fig. S1(iii)(a)), the water film thins ultimately rupturing (see Fig. S1(iii)(b)). At this stage the water level recedes owing to evaporation (see Fig. S1(iii)(c)) exposing the particle-infused surface to air. A particle shell finally emerges which loses it structural integrity with time and buckles under its own weight as depicted in (see Fig. S1(iii)(d)) as the oil it encompasses either seeps out or evaporates (albeit slower than water).

Therefore, in principle while it is true that further bursting is prevented at high particle volume fraction,  $\varphi$ , its formation is practically unproductive as it cannot form a stable oil-water mixture. This is so because, at high  $\varphi$ , initial surface coverage is high and the water surrounding the particle covered oil drop evaporates in the absence of a "protective" oil layer. We therefore restrict our attention to particle fractions which produce stable oil-water assemblies which roughly correspond to  $\varphi < 6\%$ .

# S1.1 Effect of particle size distribution on scaling relation, $N_f \sim [\varphi^{-1/4}]$ , Eq. (1) in manuscript

For our chosen clay particles the following histogram is obtained with a mean of  $\approx 15 \,\mu\text{m}$  (which is used in our theoretical scaling arguments) and standard deviation (std. dev.) of the distribution is 9.69  $\mu$ m. The coefficient of variation (COV) = std. dev./mean = 9.69/15 is 0.646 which indicates the average particle size is a good

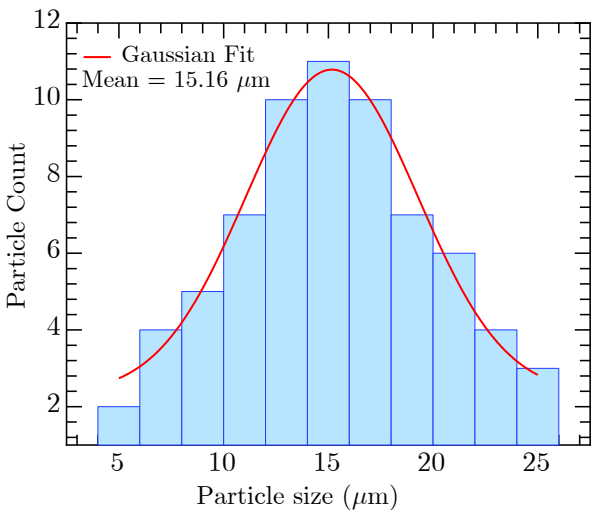
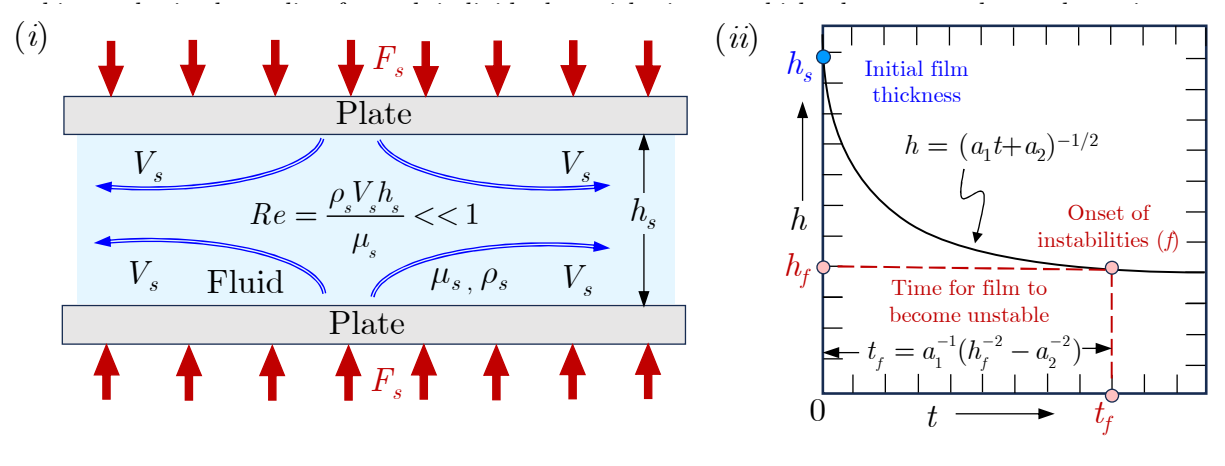


Figure S2: Particle size distribution for bentonite clay particles ( $\approx 69$  particles) as obtained from SEM image. Sample of the zoomed section is shown in Fig. 1(b) of the manuscript.

We set the premise of our reasoning by quoting our manuscript, "larger  $\varphi$  requires larger  $R_f$  with a larger surface area,  $\sim R_f^2$  to accommodate all the particles, therefore, it is reasonable to expect,  $\varphi \sim n_{c,1} \sim n_{c,f} \sim R_f^2$  thereby simplifying our scaling relation to the form,  $R_f^2 \sim \varphi$ ". To simplify this, we note that the total number of particles initially,  $n_{c,1}$  is composed of individual particles of  $n_{tot}$  (assumed without loss of generality) discrete sizes each  $a_c(j)$  in size/diameter and number, constituting a particle size distribution of the form shown in Fig. S2. Each of these particles individually initially occupy a

volume,  $V_{c,1}^{(j)}$  and surface area,  $S_{c,1}^{(j)}$  such that they constitute an individual volume fraction of  $\varphi(j)$  given by,  $\varphi^{(j)} \sim n_{c,1}^{(j)} V_{c,1}^{(j)} / \rho_o V_{drop}$  where,  $V_{drop} = (4\pi/3) R_p^3$ .

We can now apply the reasoning in the manuscript used for the entire set of particles to particles of a specific size,  $a_c(j)$ . Such a consideration means that volume fractions occupied by each of them initially and constituting a surface area, can be imagined to occupy a surface area, when the drop bursting is arrested strictly under the assumption that the initial particle size distribution remains the same. From



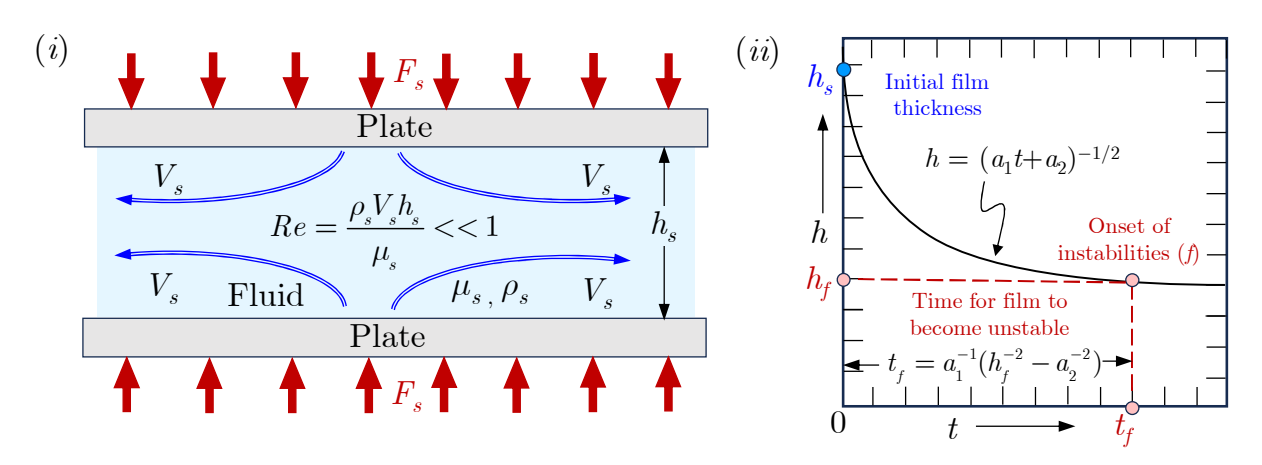


Figure S3: (i) Schematic of a typical squeeze/drainage flow problem with two forces equal in magnitude F, squeezing (s) a fluid between of density,  $\rho_s$  and dynamic viscosity,  $\mu_s$  between two plates,  $h_s$  apart (indicated by blue circles in (ii) and (iii)), at a velocity,  $V_s$  corresponding to Re << 1 and governed by Eq. S2 (ii) Dependence of dh/dt vs t as given by Eq. S5 with  $a_1 = 2F/6\mu_s R_s^4$ ,  $a_2 = h_s^{-1}$ . The time,  $t_f$ , indicated by a red circle is one at which instabilities are expected to begin manifesting themselves and is the final (f) instant of time beyond which a simple description like the one explained here is not longer applicable (iii) Dependence of h vs t as obtained in Eq. S6.

All our mathematical formulations are based on drainage flow of the bulk liquid thin film between the compound (parent) drop and the air/water interface and, the oil film between the water drop encapsulated within the (larger) oil drop. Such a situation is readily identifiable as a squeeze flow problem between in narrow gap of a given initial thickness before it is squeezed(s),  $h_s$  compressed by forces of magnitude  $F_s$  (see Fig. S3(i)) imposing a pressure, p(r,t). The lubrication equations related to low  $Re \ll 1$  flow[2] is given by,

$$\frac{dh}{dt} = \frac{1}{\mu_s r} \frac{\partial}{\partial r} \left( \frac{rh^3}{12} \frac{\partial p}{\partial r} \right) \tag{S2}$$

Assuming, h is only a function of t and not of r we can integrate Eq. S2 with respect to r noting that p is applied on a circular area with radius  $R_s$  to obtain,

$$p(r,t) = \frac{3\mu_s}{h^3} \frac{dh}{dt} \left( r^2 - R_s^2 \right)$$
 (S3)

Integrating Eq. S3 over a circular region of radius,  $R_s$ , we get,

$$F = \int_{0}^{2\pi} \int_{0}^{R_{s}} p(r,t) r dr d\theta = -\frac{3\pi}{2} \frac{\mu_{s} R_{s}^{4}}{h^{3}} \frac{dh}{dt}$$
 (S4)

From Eq. S4 the rate at which liquid is squeezed out, dh/dt can be expressed as,

$$\frac{dh}{dt} = -\frac{F_s h^3}{c\mu_s R_0^4} \tag{S5}$$

The constant c is added in Eq. S5 to account for different geometrical configurations like liquid squeezed between two plates or a sphere and a flat surface (see Section S3.1). To obtain the explicit dependence of h with t we can integrate Eq. S5 between the limits 0 to h and 0 to t to obtain,

$$h = \left(\frac{2F_s}{c\mu_s R_s^4} t + \frac{1}{h_s^2}\right)^{-1/2} \tag{S6}$$

Eq. S6, suggests that it would require infinite time to achieve rupture i.e.  $t \to \infty$  when  $h \to 0$  which is physically impossible. In practice, at a certain critical final (f) thickness,  $h_f$ , and time,  $t_f$ , the film becomes unstable and ruptures and is marked by red circles in the plot of Eq. S6 in Fig. S3(ii). Therefore, the time,  $t_f$  taken to reach  $h_f$  can be calculated by rearranging terms in Eq. S6 after setting,  $h = h_f$  as,

$$t_f = \frac{c\mu_s R_s^4}{2F_s h_s^2} \left(\frac{h_s^2}{h_f^2} - 1\right) \tag{S7}$$

In the above, it is convenient to drop the term  $(h_s^2/h_f^2) - 1$  in further analysis if  $h_f = 0.1h_s$ , which is the typical final film thickness prior to rupture in most film drainage scenarios [3]. Further, we shall use Eqns S5 and S7 developed in this section with suitable substitutions for  $F_s$ ,  $\mu_s$ ,  $R_s$  and  $h_s$  to establish the regime boundaries, (A), (B), (C), (D) and, (E).

# S3 Relation between forces and geometric variables

To accomplish our eventual goal we define,  $V_r := V_w/V_o$  and  $\rho_r := \rho_w/\rho_o$ , which help bring subsequent expressions for the different forces in their simplified dimensionless form. In so doing, we consider the mean density,  $\rho_m$  of the compound drop defined the ratio of the sum of the masses of the oil layer  $(\rho_o V_o)$  and the encapsulated water drop  $(\rho_w V_w)$  by the sum of their individual volumes,  $V_w$  and  $V_o$ ,

$$\rho_m := \frac{\rho_o V_o + \rho_w V_w}{V_o + V_w} \tag{S8}$$

By dividing the numerator and denominator of Eq. S8 by  $\rho_o V_o$  we arrive at,

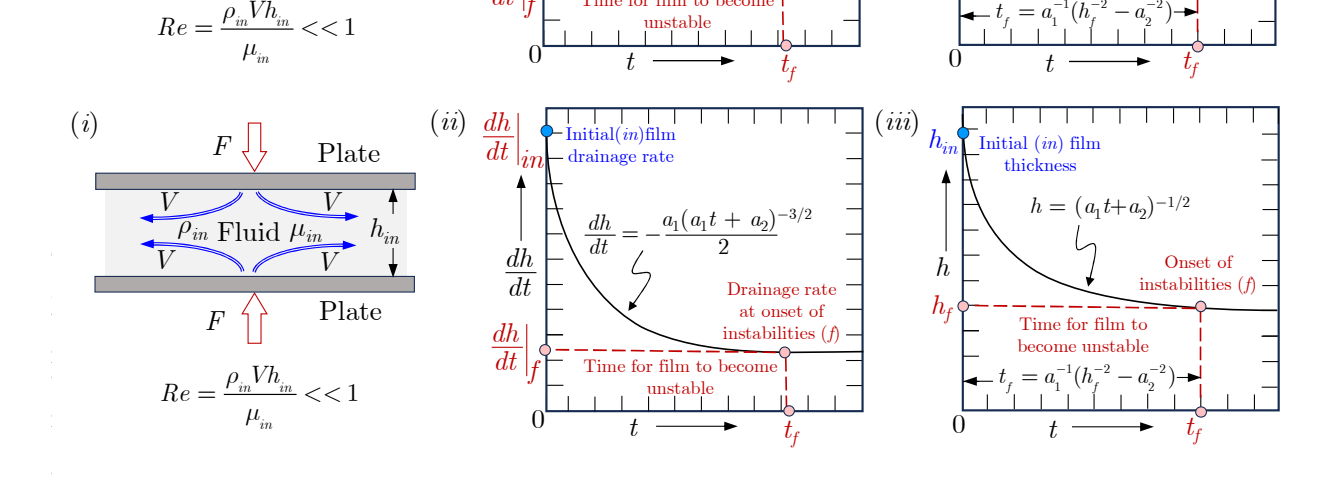
$$\frac{\rho_m}{\rho_o} = \frac{1 + \rho_{wo} V_r}{1 + V_r} \tag{S9}$$

Similarly, we can the express the parent volume,  $V_p = V_w + V_o$  in dimensionless form (by dividing both sides by  $V_o$ ) as,

$$\frac{V_p}{V_c} = 1 + V_r \tag{S10}$$

In literature, instead of  $V_r$  often the ratio of volumes  $(V_t)$  of encapsulated water  $(V_w)$  drop and parent compound drop  $(V_p)$  defined as,  $V_t := V_w/V_p$  is used. It can be related to  $V_r$  in the following manner.

$$V_t = \frac{V_w}{V_w + V_0} = \frac{(V_w/V_o)}{1 + (V_w/V_o)} = \frac{V_r}{1 + V_r}$$
 or equivalently,  $V_r = \frac{V_t}{1 - V_t}$  (S11)



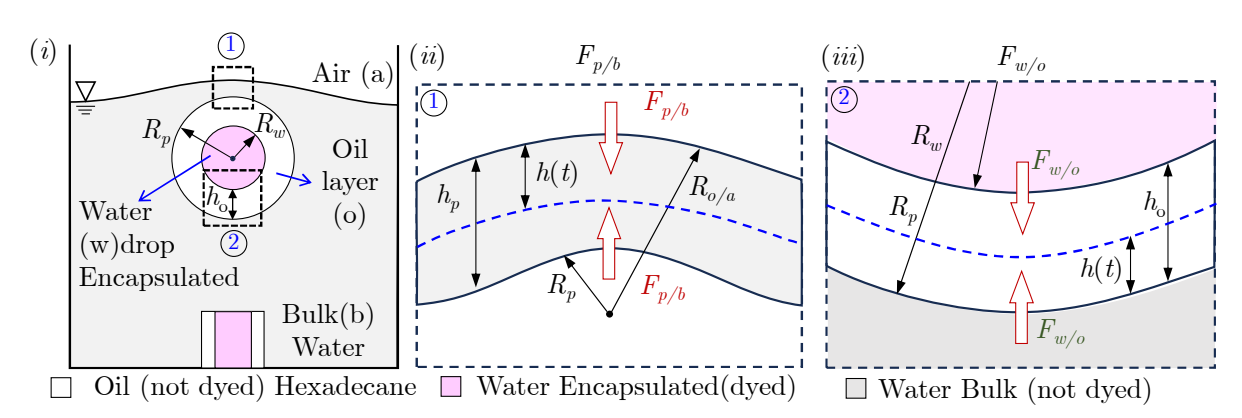


Figure S4: (i) Schematic of the setup showing the compound drop of radius,  $R_p$  with water drop of radius,  $R_w$  encapsulated within an oil (hexadecane) drop such that an oil layer of thickness,  $h_o$  is formed. (ii) Magnified v(a) of water (bulk liquid) thin film the image between the compound drop and the compound drop between the encapsulated water-drop and the compound drop-bulk water interface shown in (i) as a dotted box (iii) Magnified view of oil thin film drainage between the encapsulated water-drop and the compound drop-bulk water interface shown in (i) as a dotted box (2).

1. Expression for the spherical compound drops of mean density,  $\rho_m$  and volume,  $V_p$  is a result of the imbalance of force due its own weight (downwards),  $\rho_m V_p g$  and bupyancy/due to the displaced fluids (upwards),  $\nu_m V_p g$  drains the bulk liquid (water) shown in Figure (b)) as the magnified view of Fig. S4(i). (1). For,  $R_{o/a} > R_p$  the drainage of bulk liquid resembly atter squeeze between a sphere and a flat surface as illustrated in Fig. S5(i). Substituting fixed) Heard can see an analysis of the compound drop as,

$$\frac{F_{p/b}}{\rho_{\rm o}V_{\rm og}} = (\rho_r - 1) \tag{S12}$$

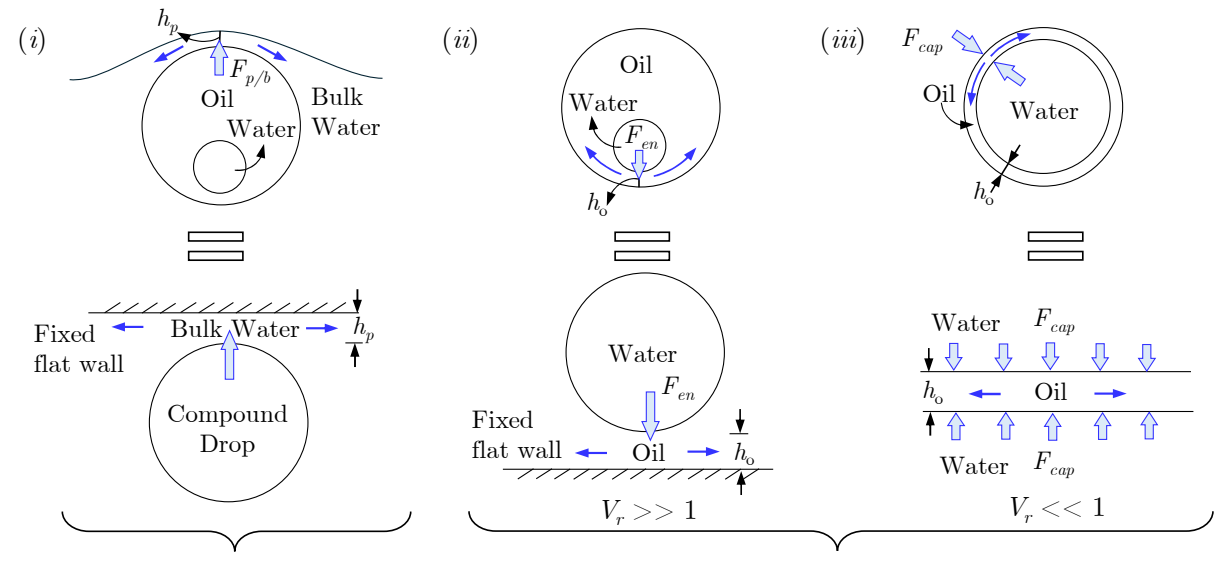
### 2. Expression for $F_{w/o}$

As the volume of the encapsulated water drop changes, the layer of oil encapsulating the water drop is reduced, consequently changing the experienced net force shown in Fig. S4(ii) as the magnified view of Fig. S4(ii) ②. In this subsection, we resolve  $F_{w/o}$  in the limits of high,  $V_r >> 1$  as  $F_{\rm en}$  and low,  $V_r << 1$  as  $F_{\rm cap}$ 

(a) When,  $V_r \ll 1$ , expression for  $F_{\rm en}$ 

During the ascent of the compound parent drop, the encapsulated water drop, owing to it higher density continually sinks inside the compound parent drop imposing a force,  $(\rho_w - \rho_o) V_w g$  corresponding to its apparent weight (accounting for buoyancy) on the intervening layer of oil. Since the compound drop also moves upwards due to buoyancy, simultaneous to the sinking of encapsulated water drop, the reduction in the oil layer gap is hastened due to application of the corresponding force given by,  $\rho_w V_p g$ . For  $R_w \ll R_p$  as is the case for  $V_r \ll 1$  the drainage flow here resembles the squeezing of flow between sphere and a flat surface as illustrated in Fig. S5(ii). The corresponding net force,  $F_{\rm en}$  imposed on this draining oil layer can be written as,

$$F_{\rm en} = (\rho_w - \rho_o) V_w g + \rho_w V_p g \tag{S13}$$



Drainage of bulk water between compound parent drop and air/bulk water interface

Drainage of oil layer between encapsulated water drop and bulk water/oil interface

Figure S5: Simplified representations for (i) bulk water thin film drainage as that of a rising sphere and a fixed flat wall since curvature of  $R_{o/a} >> R_p$ , refer Fig. S4. Oil thin film drainage at (ii)  $V_r >> 1$ , when weight of the encapsulated water drop is the dominant force and  $R_w << R_p$  (iii)  $V_r << 1$ , when capillary force,  $F_{\text{cap}}$  is dominant due to a very thin oil film,  $h_o << 1$  and  $R_w \approx R_p$ .

Substituting for  $V_p$  from Eq. S10 and definitions of  $\rho_r$  and  $V_r$  in replacing  $\rho_w$  and  $V_w$  respectively we can write,

$$\frac{F_{\text{en}}}{\rho_{\text{o}} V_{\text{og}}} = (\rho_r - 1) V_r + \rho_r (V_r + 1) = 2\rho_r V_r - V_r + \rho_r$$
(S14)

(b) When,  $V_r >> 1$ , expression for  $F_{\text{cap}}$ 

In contrast to low  $V_r$  at high  $V_r$  the oil layer thickness is sufficiently small for pressure due to capillarity to be high. Here,  $R_w \approx R_p$  as is the case for  $V_r >> 1$ , the drainage of oil resembles the squeeze flow between two flat surfaces as illustrated in Fig. S5(iii). The force,  $F_{\rm cap}$  generated due to capillarity then can be simply written as,

$$F_{\rm cap} = \sigma_{w/o} \left( 2\pi R_p \right) \tag{S15}$$

Here too, like in our previous calculations, we can make  $F_{\text{cap}}$  dimensionless by diving by  $\rho_o V_o g$  to obtain,

$$\frac{F_{\text{cap}}}{\rho_o V_o g} = \frac{3}{2} \frac{(\rho_r - 1)(1 + V_r)}{Bo_{w/o}} \quad \text{where, } Bo_{w/o} = \frac{(\rho_w - \rho_o) R_p^2 g}{\sigma_{w/o}}$$
 (S16)

#### S3.2 Relation between $h_0, R_w$ and, $V_r$

To make progress with algebra we need to express the relationships between the different geometric variables succinctly. In so doing, we note that  $R_p = R_w + h_o$  and  $V_r$  is expressed in the following manner.

$$V_r := \frac{V_w}{V_o} = \frac{\frac{4}{3}\pi R_w^3}{\frac{4}{3}\pi \left(R_p^3 - R_w^3\right)}$$
 (S17)

Eq. S17 can be further reduced using standard algebraic identities as,

$$V_r = \left\lceil \frac{R_p^3 - R_w^3}{R_w^3} \right\rceil^{-1} = \left\lceil \left( \frac{R_p - R_w}{R_w} \right) \left( \frac{R_p^2 + R_p R_w + R_w^2}{R_w^2} \right) \right\rceil^{-1}$$
 (S18)

Since,  $h_o = R_p - R_w$ , Eq. S18, the above can be rewritten in the form,

$$V_r = \left[ \left( \frac{h_o R_p^2}{R_w^3} \right) \left( 1 + \frac{R_w}{R_p} + \frac{R_w^2}{R_p^2} \right) \right]^{-1}$$
 (S19)

#### S3.2.1 Simplification when $V_r \ll 1$

At low volume fractions two deductions can be made,  $\frac{R_w}{R_p} << 1$  and  $\frac{h_o}{R_w} >> 1$ . We use these in simplifying Eq. S19 when  $V_r << 1$ .

$$V_r \approx \left[\frac{h_o R_p^2}{R_w^3}\right]^{-1} = \left[\left(\frac{h_o}{R_w}\right) \left(\frac{R_p}{R_w}\right)^2\right]^{-1} = \left[\left(\frac{h_o}{R_w}\right) \left(1 + \frac{h_o}{R_w}\right)^2\right]^{-1}$$
 (S20)

For,  $\frac{h_o}{R_{av}} >> 1$ , Eq. S20 can be reduced to the form,

$$\frac{h_{\rm o}}{R_w} \approx V_r^{-\frac{1}{3}} \tag{S21}$$

#### S3.2.2 Simplification when $V_r >> 1$

At high volume fractions two deductions can be made,  $R_w \approx R_p$  and  $\frac{h_o}{R_w} << 1$ . Similar to the previous section we use these to simplify Eq. S19 when  $V_r >> 1$  to obtain the following,

$$\frac{h_o}{R_w} \approx \frac{1}{3V_r} \tag{S22}$$

## S4 Criteria delimiting regimes of encapsulation, spreading and film bursting

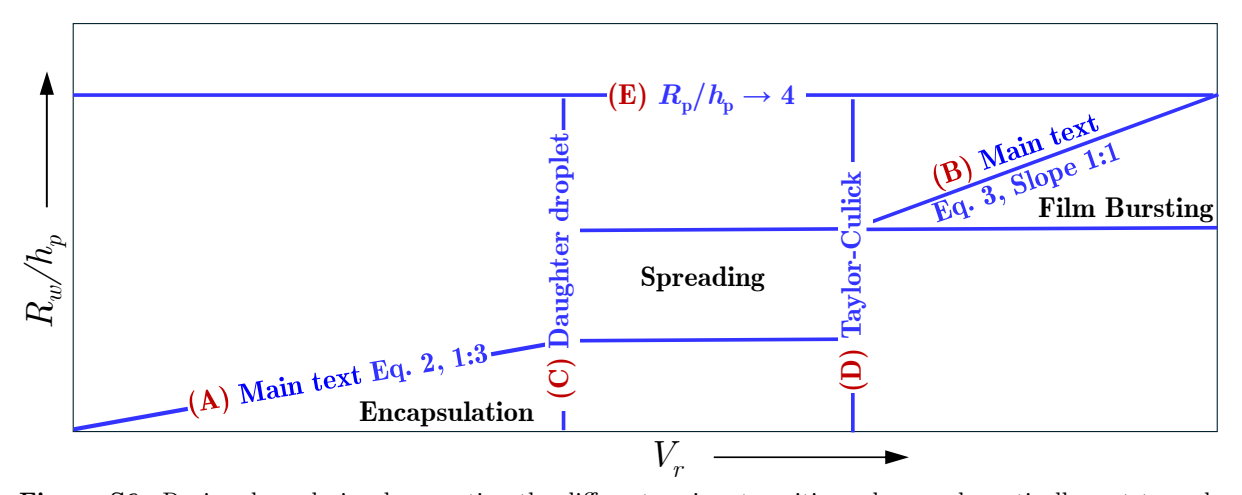


Figure S6: Regime boundaries demarcating the different regime transitions shown schematically, not to scale here and represented on log-log scale in Fig. 4 of the main text.(A) Boundary for continued encapsulation of water drop after bursting described here by Eq. S27, Section S4.1 (refer Eq. 2 of main text) (B) Boundary for onset of oil film bursting in a compound drop described here by Eq. S35, Section S4.2 (refer Eq. 3 of main text)(C) Horizontal boundary indicating cessation of encapsulation due to large daughter droplet size described here in Section S4.3, Eq. S36, (D) Horizontal limit for onset of bursting due to film bursting given by Taylor-Culick velocity, details of which are provided in Section S4.4, Eq. S37 and, (E) Vertical limit for  $R_w/h_p \to 4.4$  determined by the criterion,  $Re_b \lesssim 1$ , details of which are available in Section S4.5, Eq. S38.

# S4.1 Derivation of scaling boundary, (A), $R_w/h_p \sim V_r^{1/3}$

The fate of a compound drop (i.e. water drop encapsulated within the oil drop) after it is released from the coaxial nozzle is decided by the time scale of drainage of oil film between encapsulated of water (w) drop immersed in the oil drop,  $t_{w/o}$ , which should be slower than the time scale of drainage of water (bulk) film between between the parent compound drop (p) and the air/water interface,  $t_{p/b}$ . Mathematically, we write expressions for the two using Eq. S7 with appropriate substitutions for  $F_s$ ,  $\mu_s$ ,  $R_s$  and  $h_s$  and demand that at the boundary where daughter water droplet continues to be encapsulated within the parent oil drop after bursting,  $t_{w/o} \sim t_{p/b}$  the following should be true,

$$\frac{c_{w/o}\mu_o R_w^4}{F_{w/o}h_o^2} \sim \frac{c_{p/b}\mu_w R_p^4}{F_{p/b}h_p^2}$$
 (S23)

Or,

$$\frac{F_{p/b}}{F_{w/o}} \sim \mu_r c_s \frac{h_o^2}{h_p^2}$$
, where,  $c_s = \frac{c_{p/b}}{c_{w/o}}$  and,  $\mu_r = \frac{\mu_w}{\mu_o}$  (S24)

Before substituting for the forces,  $F_{p/b}$  and  $F_{w/o}$  above, where  $c_s$  is the ratio of drainage/thinning/squeeze (s) constants for the two configurations. We note that they can be applied only in the limit,  $V_r << 1$  when  $R_w << R_p$  and  $h_o >> R_w$ . In these conditions  $F_{w/o} = F_{\rm en}$  as derived in Eq. S14. At moderately high  $V_r$ , the expression for forces may be more complicated, containing dominant contributions from all, buoyancy, gravity and interfacial tension. However, at lower  $V_r$  this is obviated by using Eqns. S12,S14 and the assumption  $c_s \approx 1$  to transform Eq. S24 to,

$$\frac{\rho_r - 1}{2\rho_r V_r - V_r + \rho_r} \sim c_s \mu_r \frac{h_o^2}{h_p^2} = \mu_r \left(\frac{h_o^2}{R_w^2}\right) \left(\frac{R_w^2}{h_p^2}\right)$$
(S25)

Simplifying further using  $V_r \ll 1$ , we can replace  $(2\rho_r V_r - V_r + \rho_r)$  by  $\rho_r$  and substitute for  $h_o/R_w$  from Eq. S21 to arrive at the criterion below,

$$\frac{R_w}{h_p} \sim \left(\frac{\rho_r - 1}{\rho_r \mu_r^2}\right)^{1/2} V_r^{1/3}$$
 (S26)

Since  $\rho_r = 1.2$  and,  $\mu_r = 3$  are constants for our test conditions for hexadecane and water, we can write,

$$\frac{R_w}{h_p} \sim V_r^{1/3} \tag{S27}$$

Eq. S27 corresponding to Fig. 4 and Eq. 2 in the main text is determined experimentally to be of the form,  $R_w/h_p = 5V_r^{1/3}$  and shown by line (A) in Fig. S6 here.

# S4.2 Derivation of scaling boundary, (B), $R_w/h_p \sim V_r$

At high volume fractions,  $V_r >> 1$  with  $R_w \approx R_p$  and  $h_o << R_w$  or  $R_p$ . We follow the procedure in Section S4.1 however with the crucial difference that the time scale,  $t_{p/b}$  of drainage of the bulk water film between the parent compound drop (p) air/water interface should be smaller than the time scale,  $t_{\rm cap}$  of drainage of the oil layer between the encapsulated water drop and water bath (bulk) due to capillary (cap) thinning. This means the bulk water film bursts earlier, triggering perturbations which can possibly lead to bursting of the oil film sandwiched between the water bath and encapsulated water drop. In mathematical terms, using Eq. S7 this can be written as,

$$\frac{c_{w/o}\mu_{o}R_{w}^{4}}{F_{\rm cap}h_{o}^{2}} \sim \frac{c_{p/b}\mu_{w}R_{p}^{4}}{F_{p/b}h_{p}^{2}}$$
 (S28)

Or,

$$\frac{F_{p/b}}{F_{\rm cap}} \sim \mu_r c_s \frac{h_o^2}{h_p^2}$$
, where,  $c_s := \frac{c_{p/b}}{c_{w/o}}$  (S29)

From Eqs. S16 and S12 we can substitute for  $F_{p/b}$  and  $F_{cap}$  and use the approximation for  $c_s \approx 1$  to reduce Eq. S29 to,

$$\frac{(\rho_r - 1)}{\frac{3}{2} \frac{(\rho_r - 1)(1 + V_r)}{Bo_{w/o}}} \sim \mu_r \frac{h_o^2}{h_p^2}$$
(S30)

Rewriting,  $\frac{h_{\rm o}^2}{h_p^2}$  on right hand side as,  $\frac{h_{\rm o}^2}{R_w^2}\frac{R_{\rm w}^2}{h_p^2}$  we arrive at,

$$\frac{Bo_{w/o}}{1+V_r} \sim \frac{3\mu_r}{2} \frac{h_o^2}{R_w^2} \frac{R_w^2}{h_p^2}$$
 (S31)

Substituting for  $\frac{h_o}{R_w}$  from Section S3.2.2, Eq. S22 we rewrite the above inequality as,

$$\frac{Bo_{w/o}}{1+V_r} \sim \frac{3\mu_r}{2} \left(\frac{1}{3V_r}\right)^2 \frac{R_{\rm w}^2}{h_p^2} \tag{S32}$$

On rearranging the above in terms of  $V_r$  we obtain the following

$$\frac{V_r^2}{(1+V_r)} \sim \frac{\mu_r}{6Bo_{w/o}} \left(\frac{R_w}{h_p}\right) \tag{S33}$$

Finally, we use the simplification,  $V_r >> 1$  such that,  $\frac{V_r^2}{(1+V_r)} \approx V_r$ , leading us to,

$$\frac{R_w}{h_p} \sim \left(\frac{6Bo_{w/o}}{\mu_r}\right) V_r \tag{S34}$$

Like in the previous section  $\mu_r = 3$  and  $Bo_{w/o} \approx 0.45$  are constants for our test conditions for hexadecane and water, we can write,

$$\frac{R_w}{h_n} \sim V_r \tag{S35}$$

Eq. S35 corresponding to Fig. 4 and Eq. 3 in the main text is is determined experimentally to be of the form,  $R_w/h_p = 0.02V_r + 2.0$  and shown as line (B) in Fig. S6.

#### S4.3 Derivation of boundary (C), $V_r \approx 0.04$ , Daughter droplet generation limit

While the criterion given by inequality S26 sets the vertical limit for observing compound water encapsulated drops after bursting at the air/water interface, the limit on the horizontal axis of Fig. S6 corresponding to the  $V_r$  at which this may cease to occur also needs to ascertained for the regime to be bounded completely. To do so, we use the dimensionless form of the scaling relation for the daughter droplet radius,  $R_i/R_p$  produced after "i" bursting events,  $N_i$ , i.e.,  $R_i/R_p \approx N_i^{-2}$  (also stated in the main text). Setting the value of  $N_i=2$ , which corresponds to the first bursting event we obtain,  $R_2\approx R_p/4$ . The encapsulated water drop of radius,  $R_w$  must be less than the size of this daughter droplet size for perfect encapsulation to happen. Therefore we can write,  $R_w/R_p < 1/4$ . At low volume fractions,  $V_r << 1$  from Eq. S21,  $\frac{h_o}{R_w} \approx V_r^{-\frac{1}{3}}$  derived in Section S3.2.1 and noting,  $R_p = R_w + h_o$  such that,  $R_p/R_w = 1 + h_o/R_w$ , we can derive the horizontal limit, in terms of  $V_r$ , for continued water drop encapsulation in the parent compound drop after bursting as,

$$V_r < 3^{-3} \approx 0.04$$
 (S36)

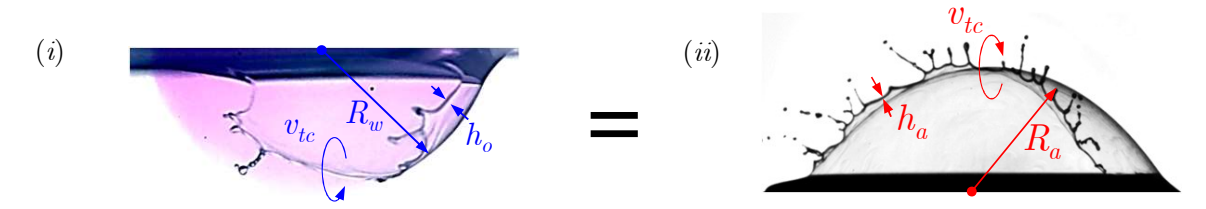
Eq. S36 corresponding to Fig. 4 in the main text is shown as the vertical line (C) in Fig. S6.

### Derivation of boundary (D), $V_r \approx 15$ , Taylor-Culick velocity limit

At moderate (mod)  $V_r$  the encapsulated drop radius,  $R_w$  is large enough so that the oil film of thickness,  $h_o$  is diminished to a size such that capillary effects dominate gravity and may be adequately described by the capillary(cap) time scale[4],  $\tau_{mod} = \left(\rho_o R_p^3/\sigma_{w/o}\right)^{1/2}$ . Herein, waves travel a distance of  $1.5\pi R_p$ , in time,  $\tau_{mod}$  at an average velocity given by,  $v_{mod}/2 = 1.5\pi R_p/\tau_{mod}$ . Once  $V_r$  increases to higher values, similar to a bursting air bubble a hole is nucleated in the oil film (see Figs. S7 (i) and (ii)) which expands, retracting at the Taylor-Culick (tc) velocity,  $v_{tc} = \sqrt{2\sigma_{w/o}/\rho_o h_o}$ . Setting,  $v_{mod}/2 = v_{tc}$  we arrive at,  $h_o/R_p = (9\pi^2/2)^{-1}$ . For,  $R_p \approx R_w$ , from Eq. S3.2.2 in Section S3.2,  $V_r \approx (h_o/R_w)^{-1}/3$  giving us the criterion above which film bursting may be observed as,

$$V_r > \frac{3\pi^2}{2} \approx 15 \tag{S37}$$

Eq. S37 corresponding to Fig. 4 in the main text is shown as the vertical line (D) in Fig. S6.



Underwater bursting oil film of thickness,  $h_o$ 

Bursting of air bubble of thickness,  $h_{\rm a}$ 

Figure S7: (i) Retraction of hole in a bursting air bubble, Lhuissier and Villermaux [5] (reprinted with permission) (ii) Retraction of a hole in a bursting underwater oil film.

# Derivation of boundary (E), $R_w/h_p \rightarrow 4.4$

The maximum value attained by  $R_w/h_p$  is when the encapsulated water drop occupies the entire volume of the compound drop, at  $V_r > 1$  equivalent to  $R_w \to R_p$ . Since the drainage flow equations mentioned in the preceding sections are only applicable after the compound drop rises to a certain distance close to the air/water interface it sets the upper limit for  $R_{II}/h_p$  (and consequently,  $R_w/h_p$ ) in our regime map. For any value above this, the bulk liquid film is expected to inconditionally stable. To ascertain this, we invoke the definition of the Reynolds number,  $Re_b := \rho_w v_w h_p/\mu_w$  and set it  $\lesssim 1$  to guarantee dominant role of viscous forces. Using this condition we may derive the expression for  $h_p$  as, Schematic cross section  $h_p \lesssim \frac{\mu_w R_{\rm Be}}{\rho_w v_w} = \frac{1}{998 \times 0.002} \approx 0.5 \text{ mm}$  (S38)

$$h_p \lesssim \frac{\mu_w R_{\text{Be}}}{\rho_w v_w} \underbrace{\text{for bother}}_{998 \times 0.002} \approx 0.5 \text{ mm}$$
(S38)

In the above we have used density of the bulk fluid made of water,  $\rho_w \approx 998 \text{ kg/m}^3$ ,  $\mu_w \approx 1 \text{ mPa-s}$  and an approach velocity,  $v_w \approx 0.002$  m/s (from our experiments). With  $h_p \approx 0.5$  mm and  $R_p \approx 2.2$  mm we get,  $R_p/h_p \approx 4$ . Since,  $R_w \approx R_p$ , we can write,  $R_w/h_p \approx 4.4$ , shown as the horizontal line (E) in Fig. S6 corresponding to Fig. 4 in the main text.

#### References

- [1] Varun Kulkarni, Venkata Yashasvi Lolla, Suhas Tamvada, and Sushant Anand. Bursting of Underwater Oil Drops. Physical Review Letters, 133(3):034004, 2024.
- [2] L Gary Leal. Advanced transport phenomena: fluid mechanics and convective transport processes, volume 7. Cambridge University Press, 2007.
- [3] Emmanouil Chatzigiannakis, Nick Jaensson, and Jan Vermant. Thin liquid films: Where hydrodynamics, capillarity, surface stresses and intermolecular forces meet. Current Opinion in Colloid & Interface Science, 53:101441, 2021.
- [4] Hiranya Deka, Gautam Biswas, Kirti Chandra Sahu, Yash Kulkarni, and Amaresh Dalal. Coalescence dynamics of a compound drop on a deep liquid pool. Journal of Fluid Mechanics, 866:R2, 2019.
- [5] Henri Lhuissier and Emmanuel Villermaux. Bursting bubble aerosols. Journal of Fluid Mechanics, 696:5-44.